Dosimetry formalism and calibration procedure for electronic brachytherapy sources in terms of absorbed dose to water

Abdullah Abudra'A, Bruno Chauvenet, Jean Gouriou, Johann Plagnard, Itti Ramona, Isabelle Aubineau-Lanièce

Dosimetry formalism and calibration procedure for electronic brachytherapy sources in terms of absorbed dose to water

A. Abudra'a[1], B. Chauvenet[1], J. Gouriou[1], J. Plagnard[1], R. Itti[2], I. Aubineau-Lanièce[1]

[1]CEA, LIST, Laboratoire National Henri Becquerel (LNE-LNHB), CEA Saclay, 91191 Gif-Sur-Yvette Cedex, France

[2]Service de cancérologie – Radiothérapie, Hôpital Saint Louis, 1 Avenue Claude Vellefaux, 75010 Paris, France

isabelle.aubineau-laniece@cea.fr

Abstract. The LNE-LNHB has developed a methodology to standardize electronic brachytherapy sources in terms of absorbed dose to water. It is based on the measurement of the air-kerma rate at a given distance from the source and the Monte Carlo calculation of a conversion factor. This factor converts the air kerma in measurement conditions into absorbed dose to water at a 1 cm reference depth in a water phantom. As a first application, the method was used to calibrate a Zeiss INTRABEAM system equipped with its 4 cm diameter spherical applicator. The absorbed-dose rate value obtained in the current study was found significantly higher than that provided by the manufacturer in line with the observations already reported by a few other teams.

1. Introduction

Electronic brachytherapy (eBT) is a cancer treatment technique using low-energy x-rays ($\leq$ 70 keV). A variety of clinical systems are now available for treatment, each of them being equipped with a miniature x-ray generator and removable applicators adapted to the type and size of tumors. There are currently a few hundred eBT systems in use worldwide. Among them, one can cite Papillon 50 (Ariane Medical Systems Ltd), Xoft Axxent (iCAD Inc.), Esteya (Elekta AB-Nucletron), Photoelectric therapy (Xstrahl Ltd), SRT-100 (Sensus Healthcare) and INTRABEAM (Zeiss) (Eaton *et al* 2010).

To deliver the prescribed dose to patients using such devices, medical physicists rely today on the databases provided by the manufacturers. For most systems, there is a lack of dosimetric data independent of suppliers, hence metrological traceability is needed. So far, the dosimetric quantity recommended to characterize radiotherapy radiation sources is absorbed dose to water. The depth in water of the reference point as specified by AAPM (TG-43) for brachytherapy is 1 cm (Rivard et al 2004), while those specified by AAPM (TG-61) and IAEA (TRS 398) are at surface for low-energy x-ray beam dosimetry (< 100 kV), and 2 cm for medium-energy x-ray beam dosimetry (> 100 kV) (Ma *et al* 2001, IAEA 2000). By extension to novel brachytherapy applications, the depth of 1 cm in water for the reference point seems generally accepted for electronic brachytherapy (Eaton 2015).

The NIST has established an air-kerma standard for low-energy electronic brachytherapy sources based on its Lamperti free-air chamber, presented in (Seltzer *et al* 2014) with the characterization of an Xsoft Axxent source. The PTB is developing a dedicated extrapolation ionization chamber as primary standard instrument for absorbed-dose-to-water measurements (Schneider *et al* 2016). Regarding the INTRABEAM system, besides the manufacturer's documentation, several works describing dosimetry measurement methods have already been published. One of them (Eaton *et al* 2010) is based on the IPEMB code of practice

(Klevenhagen *et al* 1996). Recent publications from the Medical Physics Unit of the McGill University present results based on the use of a cavity ionization chamber calibrated in terms of air kerma with an associated Monte Carlo calculated conversion factor. This factor converts the air-kerma calibration coefficient into one in terms of absorbed dose to water ("C_Q formalism"). Complementary results based on calibrated EBT3 Gafchromic film measurements are also presented (Watson *et al* 2018a, Watson *et al* 2018b).

In the present work carried out mainly in the frame of a thesis (Abudra'a 2017), a measurement method has been studied to standardize eBT sources in terms of absorbed dose to water at 1 cm depth. Considering a priori that a national metrology laboratory cannot be equipped with all the systems commercially available, the developed methodology was aimed at being general enough to be applicable to any such system.

The INTRABEAM system supplied by the Zeiss company was chosen for a first application since it is the most widespread electronic brachytherapy system in France. Its main use is in intraoperative radiotherapy treatments (IORT) of breast cancer for which spherical applicators of various diameters are used. The present paper focused for a first approach on the spherical applicator of 4 cm in diameter, the method being applicable to any other applicator.

2. Methods and materials

2.1. Method

The methodology consists first in selecting, or if needed in establishing, a primary reference in terms of air-kerma rate in an x-ray beam of the laboratory with a quality close to that delivered by the eBT device. A transfer cavity ionization chamber calibrated in this beam is then used on site at the hospital to measure the air-kerma rate delivered by the eBT device at an appropriate distance in air. Finally, the absorbed-dose rate to water in reference conditions is derived from the measured air-kerma rate using a calculated conversion factor.

In more details, the method can be decomposed into the following steps:

1) characterization of the photon energy spectrum of the considered eBT device in the chosen configuration (for example, bare or associated with an applicator);
2) selection of the reference beam to be used for the calibration in air-kerma of the transfer cavity ionization chamber chosen for characterizing the photon beam of the eBT device:
    a) choice, if available, of the most appropriate x-ray reference beam of the laboratory;
    b) otherwise, realization and characterization in terms of air-kerma rate of a new reference beam with an appropriate energy spectrum;
3) air-kerma calibration of the transfer chamber in that reference beam;
4) derivation of the calibration coefficient of the transfer chamber for the beam quality of the eBT device in the same irradiation conditions as the reference beam;
5) Monte Carlo calculation of the factor F_{KD} that converts the air kerma at the measurement point in the eBT beam into absorbed dose to water in the reference conditions;
6) on-site measurement of the air-kerma rate delivered by the eBT device using the calibrated transfer chamber and derivation of the absorbed-dose rate to water at the reference point, applying the conversion factor F_{KD}.

At step 2, the air-kerma rate at the reference distance is measured with a primary standard free-air ionization chamber (FAC) in the reference beam, using the classical formula (Burns *et al* 2011):

$$\dot{K}_{\mathrm{air,ref}} = \frac{W_{\mathrm{air}}}{e} \cdot \frac{I_{\mathrm{FAC}}}{\rho_{\mathrm{air}} V_{\mathrm{FAC}}} \cdot \frac{1}{1-g_{\mathrm{air}}} \cdot \prod_{\mathrm{i}} k_{\mathrm{i}} \qquad (1)$$

where W_{air} is the mean energy expended by an electron to produce an ion pair in air; e is the elementary charge; V_{FAC} is the FAC measurement volume; ρ_{air} is the air density in the reference atmospheric conditions of the laboratory (1013.25 hPa, 20 °C and 0% relative humidity); I_{FAC} is the net ionization current measured with the FAC in the reference beam (ionization current corrected for background, temperature, pressure and humidity, polarity and recombination);

g_{air} is the fraction of the initial electron energy lost through radiative processes in air; $\prod_{\mathrm{i}} k_{\mathrm{i}}$ is the product of correction factors relating to the FAC.

The accurate knowledge of the photon energy spectrum of the reference beam is required to calculate those correction factors. Accuracy is all the more critical as the energy is low, because of the steep variation of photon interaction coefficients below some tens of keV, and of their differences between air and chamber constituent materials.

To select an appropriate reference beam, one has to estimate the required degree of similarity of its energy distribution compared to that of the eBT beam. This depends on the characteristics of the chosen transfer ionization chamber, especially its energy response. The flatter this response, the lower the effect of the energy-distribution differences. In practice, this involves evaluating the beam quality correction factor of the chamber, $k_{Q,Q\mathrm{ref}}$ and its uncertainty, with Q_{ref} and Q the qualities of the reference and eBT beams respectively.

At step 3, the calibration coefficient of the transfer chamber in the reference beam can be expressed by:

$$N_{K_{\mathrm{air,ref}}} = \frac{\dot{K}_{\mathrm{air,ref}}}{I_{\mathrm{TC,ref}}} = \left[\frac{W_{\mathrm{air}}}{e} \cdot \frac{I_{\mathrm{FAC}}}{\rho_{\mathrm{air}} V_{\mathrm{FAC}}} \cdot \frac{1}{1-g_{\mathrm{air}}} \cdot \prod_{\mathrm{i}} k_{\mathrm{i}}\right] \cdot \frac{1}{I_{\mathrm{TC,ref}}} \qquad (2)$$

where $I_{\mathrm{TC,ref}}$ is the net ionization current of the transfer chamber measured in this beam.

At step 4, the air-kerma calibration coefficient for a beam quality equal to that of the eBT beam is derived from relation (2) multiplying it by the beam quality correction factor $k_{Q,Q\mathrm{ref}}$.

$$N_{K_{\mathrm{air,eBT}}} = \frac{\dot{K}_{\mathrm{air,ref}}}{I_{\mathrm{TC,ref}}} k_{Q,Q\mathrm{ref}} \qquad (3)$$

At step 5, it is worth noting that the calculated conversion factor F_{KD} depends only on the characteristics of the eBT beam, and not on the transfer chamber used.

Finally, at step 6, the rates of air kerma at the measurement distance and of absorbed dose to water at the reference depth can be expressed respectively by:

$$\dot{K}_{\mathrm{air,eBT}} = N_{K_{\mathrm{air,eBT}}} \cdot I_{\mathrm{TC,eBT}} \cdot k_{\mathrm{dis}} \cdot k_{\mathrm{stem}} = \dot{K}_{\mathrm{air,ref}} \cdot \frac{I_{\mathrm{TC,eBT}}}{I_{\mathrm{TC,ref}}} \cdot k_{Q,Q\mathrm{ref}} \cdot k_{\mathrm{dis}} \cdot k_{\mathrm{stem}} \qquad (4)$$

$$\text{and } \dot{D}_{\mathrm{w}} = \dot{K}_{\mathrm{air,eBT}} \cdot F_{\mathrm{KD}} \qquad (5)$$

$I_{\mathrm{TC,eBT}}$ is the net ionization current of the transfer chamber measured in the eBT beam at the measurement distance in air. k_{dis} corrects for the evaluation of the distance between the eBT photon source and the transfer chamber. k_{stem} is the transfer-chamber stem correction factor due to the difference between the reference and eBT beam sizes at the points of measurement, resulting in different contributions of radiation scattered in the body and stem of the chamber.

2.2. Materials

2.2.1. Selected eBT device

To test its feasibility, the method was applied to the Zeiss INTRABEAM system. This system is a compact mobile x-ray source. The electrons emitted by the heated cathode wire are accelerated to a potential of 50 kV (a 40 kV potential is also accessible) and collimated using an electromagnetic deflector. The resulting electron beam is then guided through a cylindrical probe to a thin gold target layer covering the inner surface of the hemispherical probe tip. Finally, the interactions of electrons with the gold target lead to the production of x-rays in an approximately isotropic 4π sr distribution.

This cylindrical probe source was originally used in the treatment of brain tumors in the 1990s. It has been subsequently used for other indications after the development of its applicators. Those applicators of different sizes and shapes allow to treat different types of cancer, i.e. gastrointestinal, spinal metastasis and skin. The treatment times depend on the chosen applicator size and prescribed dose (10-20 Gy to tissue at contact of the applicator) and vary between 2 and 50 minutes.

Since 1998, it is primarily used for the IORT of breast cancer (Kraus-Tiefenbacher *et al* 2005). For such treatment, spherical applicators are inserted into the cavity left by the tumor excision. They are made of biocompatible polyetherimide material, whose density ranges from

1.27 g/cm^3 to 1.51 g/cm^3. To give a good conformance of the applicator surface to the tumor cavity, their outer diameters range from 1.5 cm to 5 cm, by steps of 0.5 cm. The applicator is mounted on the x-ray source, the probe being inserted in its inner cavity. For ensuring the reproducibility of positioning, the applicator is attached to it with a metal ring in stainless steel added to its shank end.

In the present work, the INTRABEAM x-ray source of Saint-Louis Hospital (Paris) was studied associated with a 4 cm-diameter spherical applicator.

2.2.2. Monte Carlo code

The Monte Carlo code used for calculating the photon energy spectra and the conversion factor F_{KD} was the version 2006 of the PENELOPE code (Salvat *et al* 2006). More specifically this was a version modified for working in parallel computing and chosen for this reason despite the existence of more recent versions of PENELOPE. Several parameters can be varied to adjust the mixed procedure for electron tracking, i.e. the mean free path between hard elastic events (C_1), the maximum average fractional energy loss in a single step (C_2) and the cutoff energies of inelastic collisions (W_{CC}) and bremsstrahlung emission (W_{CR}). In all the calculations made in the present work, the recommended values of 0.05 were assigned to C_1 and C_2, W_{CC} and W_{CR} were both set at 1 keV, as well as the absorption energy parameters (E_{abs}) which define for each material and particle type the energy threshold below which particle tracking is stopped and the particle energy absorbed. That energy was chosen because at 1 keV, the photon mass attenuation coefficients in air and water are very high, around 4×10^3 cm^2/g. Therefore the photons at that energy or less are locally absorbed in water and absorbed at 99% in air after crossing 1 cm. Then the only photons of 1 keV or less present in water or air at the measurement distance are secondary photons produced by interactions of photons of higher energies, and thus their fluence becomes very low. Finally, the parameter DSMAX which controls the maximum step length of electrons and positrons in a given body was set at the recommended value of one

tenth of the corresponding body thickness. This parameter was applied to all the volumes (constitutive parts of the eBT probe, applicator and scoring region) in the calculation of the phase-space data files described in subsection 2.2.3, and only to the scoring regions in the other calculations.

2.2.3. Monte Carlo modelling of the INTRABEAM probe

The Monte Carlo model of the INTRABEAM probe relies on data delivered by ZEISS or found in publications (Yanch *et al* 1996, Nwanko *et al* 2013) (figure 1). The probe length is 10 cm and its outside diameter is 3.2 mm (without the three external biocompatible layers further described). The thickness of the gold target is taken equal to 1 μm (Beatty *et al* 1996). The tip of the probe shaft is made of beryllium that works as a transparent x-ray window, over a length of 2 cm. The remaining part is made of μ-metal (a nickel-iron alloy composed of at least 75% of nickel) of 0.5 mm thickness to provide rigidity and shielding against static or low-frequency magnetic fields. In our model, μ-metal was replaced by nickel alone for the sake of simplicity due to a lack of information on the other constituent materials (figure 1). This approximation was assumed to have a negligible impact on the calculated outgoing photon fluence due to the very small solid angle (around 1.6×10^{-3} sr) under which this part of the probe is seen from the photon source (gold target). The entire probe is coated with three thin layers of materials ensuring durability and biocompatibility with tissues. The model includes those layers of 2.5 μm thickness each and made, from the inside to the outside, of NiO, Ni and CrN (Nwankwo *et al* 2013).

The electron beam hitting the gold target is reported to be approximately Gaussian, oscillating around the central axis in order to optimize the isotropy of the radiation field (Beatty *et al* 1996; Yanch *et al* 1996). The interactions of electrons in the target give rise to 16 bremsstrahlung emission sources, disk-shaped and equidistant (Sievers *et al* 2011, Sievers 2012). To reproduce them in the model, 16 disk-shaped electron sources located at the base of the modelled probe

were introduced (figure 2). The electrons were emitted uniformly from each disked-shaped source with a Gaussian energetic distribution of 50 keV mean value and 1.06 keV standard deviation, and directed towards the target along the probe and parallel to it.

A 4 cm spherical applicator made of polyetherimide (PEI) was measured by radiography for this study. Its internal cavity has a radius of 2.8 mm. It is filled with a volume of air surrounding the probe inside the applicator. The Monte Carlo model of the probe with its applicator is shown in figure 3. The parameters of the materials present in the model of the eBT probe and those introduced for air-kerma and absorbed-dose-to-water calculations are reported in Table 1. They were based on the PENELOPE-pendbase materials database, being either directly obtained using the material reference number in that database, or composed from their chemical formula.

Table 1. Parameters of the materials present in the modelled eBT probe and air-kerma and absorbed-dose calculations.

Material	Au	Be	NiO	Ni	CrN	PEI	Dry Air (20 °C)	Pb	Al	Plexiglas	Water (4 °C)
Reference # in pendbase	79	4	-	28	-	-	104	82	13	224	278
Density (g/cm^3)	19.32	1.848	6.67	8.902	5.9	1.4	1.20479×10^{-3}	11.35	2.6989	1.19	1

Information on particles leaving the applicator was made available by generating six phase-space (phsp) data files using as scoring region a 10 µm-thick spherical-shell volume surrounding the surface of the applicator. The calculations were performed without any variance reduction techniques under the same configuration with different initial seeds, reaching a total size of 120 gigabytes corresponding to about 1.4 billion scored particles.

2.2.4. Photon spectrometry system

An advantage of determining an x-ray energy spectrum using photon spectrometry is that it is based on the actual beam. For its part, the calculation relies on a modelled source for which there is often a lack of detailed information about x-ray tube components and their possible deterioration with time. The interest of doing both is cross validation. Due to the large use and

impact of Monte Carlo calculations in the method applied, it is of particular interest to have the possibility to validate the modelling of the x-ray source and the calculation of the energy distribution of produced x-rays.

The spectrometry system used for the experimental determination of photon energy distributions was previously developed at LNHB (Plagnard 2014, Deloule 2014, Plagnard 2016). This system consists of a CdTe semiconductor detector connected to a digital signal processing module LYNX supplied by Canberra for spectra acquisition. In-house developed algorithms were applied to correct for the distortions of measured spectra caused by artifacts associated with detection processes, i.e. pulse pile-up, fluorescence x-ray photon escape, intrinsic detector efficiency, etc. Here fluorescence escape mainly concerns K-shell fluorescence x-ray photons of cadmium and tellurium emitted after photo-electric interactions that occur in the CdTe detector. The minimum energy to create them is 26.7 keV for cadmium and 31.8 keV for tellurium. Moreover, in order to limit the high count rate generated by the incoming photon flux and so pile-up distortion, a very small solid angle (less than 5×10^{-5} sr), resulting from an optimal layout of the source-to-detector distance and small collimation (in the order of hundreds of micrometers in diameter), is adapted for each measurement. To ensure the correct alignment of the collimator on the beam axis, a specific automatic positioning system was developed which includes two automatic rotation stages and a devoted Labview program. This positioning system enables to find and then adjust the position on the source-detector axis corresponding to the highest count rate. The device set up for the on-site spectrometry measurement of the eBT system is shown in figure 4.

2.2.5. Reference x-ray generator

The Gulmay x-ray generator (160 kV) of the laboratory, serving as radiation source for low-energy x-ray references, was used with a high voltage set at 50 kV. Since the anode of that x-ray generator is made of tungsten instead of gold, the energies of the fluorescence photon peaks

(7 keV-12 keV) are different, and so the photon energy spectrum of the INTRABEAM bare probe cannot be strictly reproduced using this generator. However, due to their low energy, the fluorescence photons are strongly attenuated through the spherical applicator with an additional filtration equivalent to 1 cm of water, the chosen reference depth. Thus, the accurate reproduction of the eBT photon spectrum in this configuration becomes quite feasible.

2.2.6. Transfer ionization chamber

The model of transfer chamber chosen for standardizing the eBT device was the PTW-23342, a plane parallel chamber of small sensitive volume (0.02 cm^3). This chamber is characterized by its flat energy response (see Table 8.1 in IAEA (2000)). A chamber of this type is also used by Zeiss for the dosimetric characterization of their INTRABEAM system using their TARGIT method. Measurements were carried out here with two PTW-23342 chambers associated with a MAX-4000 electrometer. Both chambers were calibrated in terms of air kerma using relation (2). In the calibration conditions, their body was fully irradiated, the beam diameter being equal to 9.5 cm at the reference point.

The positioning system used for the measurements made on site at St. Louis Hospital (Paris) is shown in figure 5. A collimation device in lead was mounted around the eBT x-ray source to get rid of a possible contribution of photons backscattered from the surrounding materials.

3. Results

3.1. Comparison of measured and calculated spectra of the eBT source

The spectrometry experimental setup was adapted to measure the photon energy spectra on the probe axis of the eBT device with or without spherical applicator (figure 4). The source-detector distance was 50 cm, i.e. the usual reference distance in the x-ray reference beams of the laboratory. To characterize the spectra obtained after different layers of water, the first solution was to immerse the probe in a cylindrical container in Plexiglas (60 mm in diameter, 100 mm high and 2 mm thick) filled with water, enabling to reach given water-equivalent thicknesses,

taking account of the container bottom thickness (figure 4, left and middle). Micrometric positioning systems (translation stages providing 10 µm steps) and an optical laser were used for precise source-detector alignment and distance measurements. For all the measurements, the collimation at the detector entrance window was characterized by a diameter of 500 µm. Further measurements were performed using aluminium filters instead of a water-filled container (figure 4 right). In practical terms, their use has several advantages, such as simpler measurement process, suppression of the uncertainty of container bottom thickness and elimination of the difficulty to attain the nominal distance between the applicator sphere surface and the container bottom (*t* in figure 4, left). Spectra obtained with water-filled containers or aluminium (Al) filters were measured for increasing thicknesses, by steps of 5 mm up to 40 mm for water, and by steps of 0.35 mm up to 2.8 mm for Al (figure 6). The peaks in the low-energy part of the spectra (10 keV-14 keV) presented in figure 6 correspond to the L-shell fluorescence photons of the gold anode target of the eBT source. Being major components of the bare-probe spectrum (figure 7), they progressively vanish with increasing thickness of absorbing material (figure 6), and become undetectable when adding a 1-cm thick layer of water (figure 6, black curves). The fluence-averaged energies range from 30.0 keV for 0.35 mm Al up to 34.1 keV for 2.8 mm Al. An Al filter of 0.7 mm was found equivalent to 1 cm water in terms of attenuation for the considered photon energy distribution.

Measured energy spectra were compared with calculated ones for several configurations and found to be in agreement. For example, regarding the measured and calculated spectra obtained with a 0.7 mm Al filter on the probe axis of the eBT device (figure 6, black continuous line and triangles, respectively), their fluence-averaged energies were respectively 30.9 keV and 31.2 keV. Due to the uncertainties associated to the modelling of the eBT source and to the actual energy of accelerated electrons in the probe, this difference of 0.3 keV can be considered as insignificant. From the compared characteristics of the beams presented in Table 2 in terms

of Al filtration, of fluence-averaged energy and HVL, it can be estimated by interpolation that this corresponds to a change in HVL value of approximately 0.07 mm.

3.2. Realization and characterization of the X-ray reference beam

3.2.1. Choice of the INTRABEAM irradiation conditions for air-kerma measurements

It is of interest to choose measurement conditions of air kerma such that the calculations of that quantity and absorbed dose to water at 1 cm depth present in the conversion factor F_{KD} be strongly correlated. This should reduce the type-B uncertainty of F_{KD}. Thus it was decided to standardize in air kerma the eBT source with a 4 cm applicator and a 0.7 mm-thick Al filter (equivalent to 1 cm of water), at a large distance from the source. The photon fluence at the measurement point is then almost exclusively composed of primary photons, whose energy distribution is modified by the attenuation through the applicator, the Al filter, and negligibly air. This effect on the photon fluence is almost the same as the effect of the absorption of primary photons through the applicator and the 1-cm thick layer of water surrounding it in water. However, there is in water the additional contribution of scattered and backscattered photons, that is negligible in air. This difference is reflected in the shapes of the photon spectra in air and in water, calculated respectively at the measurement point (as defined in section 3.3.2) and at the reference point (figure 8). The energy distribution in water remains almost unchanged below 20 keV but is significantly distorted above, due to the high number of interactions in water, predominantly Compton above 30 keV. The resulting photon fluence-averaged energy at 1 cm in water is 30.4 keV, slightly lower than the one obtained in air with a 0.7 mm Al filter, 31.2 keV (section 3.1).

3.2.2. Realization of the X-ray reference beam

The second step of the method deals with the choice of an appropriate reference beam for the calibration of the transfer ionization chamber, involving if needed the realization of a new one. The method aiming at being applicable to a large variety of transfer chambers, and not only

those used here, it is then of interest to examine the possible ways to evaluate the influence of differences in photon energy spectra on the response of a transfer ionization chamber. The simplest one is to compare the air-kerma calibration coefficients of the chamber in two existing reference beams that frame the medical eBT beam in terms of energy. In case of negligible or very small deviation, it can be sufficient to calibrate this chamber in one of these beams, the beam quality correction factor $k_{Q,Q\mathrm{ref}}$ being taken equal to 1 with an uncertainty evaluated from that deviation. When the energy response of the chamber and the energy spectra of the beams are known, a more rigorous solution can be applied. The calibration coefficient of the chamber can then be calculated and the beam quality correction factor $k_{\mathrm{Q,Qref}}$ is then derived from the ratio of the so calculated calibration coefficients. The calculated quantities of the numerator and denominator being close, the resulting uncertainty should be reduced due to strong correlations between them. This method applicable to any type of chamber, regardless the flatness of its energy response, allows to be less restrictive in the choice of reference beams and transfer chambers, as long as the uncertainty of the calculated factor $k_{\mathrm{Q,Qref}}$ remains acceptable. When none of those methods can be used, there remains the alternative of step 2b (section 2.1).

Both steps 2a and 2b (section 2.1) have then been applied in the present work. In addition to the existing CCRI50b reference beam, two new reference beams were realized reproducing the eBT source with a spherical applicator (one of 4 cm diameter, and the other of 3 cm diameter) and a 1-cm thick layer of water or an equivalent 0.7-mm Al filter.

The shapes of the measured and calculated spectra of the eBT device and of the x-ray generator with selected filtrations are in good agreement (figure 9). For spectrometry measurements, a low generator current (0.5 mA) was used to decrease the photon flux and hence the pulse pile-up effect in raw measurement spectra, assuming no significant influence of current intensity on the energy of x-rays. The distance between the detector window and the tungsten anode of the x-ray generator was 50 cm, the usual reference distance.

The spectrum obtained with the 3 cm spherical applicator is harder than with the 4 cm one; this results from the presence of an extra internal aluminum filter inside the applicators of diameters of 3 cm and less. The characteristic parameters of those spectra are summarized in Table 2. For comparison, the CCRI 50b beam is obtained with an Al filter thickness of 1.057 mm, its Al half-value layer (HVL) being equal to 1.013 mm.

In that table, the ratio of the values of the "air kerma per unit fluence" in the eBT and reproduced beams is given to compare them. This quantity can be expressed as follows:

$$K_{\mathrm{air}}/\Phi = \frac{\int_0^{E\max} E\,\Phi_E(E)\left(\frac{\mu_{\mathrm{tr}}(E)}{\rho}\right)_{\mathrm{air}} \mathrm{d}E}{\int_0^{E\max} \Phi_E(E)\,\mathrm{d}E} \qquad (6)$$

where Φ is the total photon fluence, Φ_E is its energy distribution and $\left(\frac{\mu_{\mathrm{tr}}(E)}{\rho}\right)_{\mathrm{air}}$ the mass energy transfer coefficient of air. Requiring the knowledge of the shape of the energy spectrum, this quantity could be used as a quality index for x-ray beams characterized in terms of air kerma. For metrological purpose, it should be more sensitive and specific than the half-value layer (HVL) of Al combined or not with the tube potential (kV), that can give insufficient information for some dosimetry applications (Ma *et al* 2001).

Table 2. Characteristic parameters of the photon spectra of the INTRABEAM with a 4 cm or a 3 cm spherical applicator, and 1 cm water-equivalent filter, and of the reproduced beams.

		4 cm applicator + 1 cm water	3 cm applicator + 1 cm water
Filter thickness added for the reproduced beam (mm Al)		1.715	2.484
Fluence-averaged energy (keV)	INTRABEAM	30.9	32.1
	Reproduced	30.7	32.1
HVL (mm Al)		1.369	1.712
Ratio of air kermas per unit fluence INTRABEAM/reproduced (Cf. relation (6))		0.996	1.001

3.2.3. Characterization of the reference beam in terms of air kerma

The air-kerma reference values were measured using the air-kerma standard free-air ionization chamber of the laboratory dedicated to low-energy x-rays. The measurement and determination of correction factors were carried out in the same way as for formerly established references, using formula (1) (Burns *et al* 2011). In this relation, the term $\prod_i k_i$ can be detailed as the product of correction factors for electric field distortion (k_d), air attenuation (k_a), electron loss (k_e), scattered radiation (k_{sc}) (including fluorescence), diaphragm effects and wall transmission (k_{dia}). Except for k_d, those factors are determined from Monte Carlo pre-calculated values obtained for mono-energetic photons at regular intervals and, for k_a, on values taken from the XCOM database, by calculating their weighted summations over the photon energy spectrum of the beam. For the beam reproducing the eBT source with the 4 cm applicator, the product of those correction factors, obtained with a relative standard uncertainty of 0.12%, was found 0.18% lower than for the CCRI50b beam. The additional product of correction factors k_{ii} k_w for the initial ion pair and energy dependence of W_{air} here found equal to 0.9978(5) was included using the table of values given in the ICRU Report 90 (ICRU 2016). Accounting for the increase of the standard uncertainty of W_{air} newly recommended in that report (0.35% instead of 0.15%), the air-kerma rate was determined with a relative standard uncertainty of 0.45% (see Table 3).

Table 3. Uncertainty budget of the air-kerma reference.

Quantity	**Uncertainty (%, k = 1)**
I_{FAC}	0.24
W_{air}/e	0.35
ρ_{air}	0.01
V_{FAC}	0.08
$1/(1\text{-}g_{air})$	0.01
$\prod_i k_i$	0.12

Product	**0.45**

3.3. Dosimetric characterization of the eBT x-ray source

3.3.1 Transfer ionization chamber calibration

To evaluate the impact of the photon energy distribution on the calibration coefficient, one of the two chambers was calibrated in the three reference beams described above. As expected for this chamber, no significant difference was observed between those calibration coefficients (figure 10). In the studied case, the step 2a of the method is sufficient and quite appropriate, choosing the CCRI50b beam as reference beam with a negligible or very small increase in uncertainty.

3.3.2 Air-kerma rate measurements with the transfer chamber

The low sensitivity (around 1 nC/Gy) of the transfer chambers imposes relatively short measurement distances in the eBT beam. The measured current drops dramatically with increasing source-to-detector distance, thus increasing the measurement uncertainty. On the other hand, the relative uncertainty due to positioning increases when bringing the chamber closer to the source. A compromise has then to be found between those two effects. In this work, the measurement point, taken on the inner surface of the chamber entrance window, was located at a distance of 13.55 cm from the external surface of the bare probe tip. Given the experimental conditions described above, a standard uncertainty equal to 0.33 mm was assigned to the chamber position, leading to a relative uncertainty of 0.5% on the distance correction factor k_{dis} taken equal to 1.

The beam size at the measuring point was determined both by Monte Carlo simulation and experiment using a Gafchromic^{TM} EBT3 film. A diameter of 3.5 cm was found, ensuring full irradiation of the chamber cavity but only a partial one of its body. The measured current had then to be corrected for the effect of beam size difference compared to calibration conditions.

The corresponding factor k_{stem} was evaluated from experimental results reported in (Seuntjens 2000, figure 3) and found equal to 1.008 with a standard relative uncertainty of 0.1%. Due to the close similarity of calibration and measurement x-ray energy spectra, the factor $k_{Q,Qref}$ was taken equal to 1 with a relative standard uncertainty less than 0.1%.

The air kerma rates were obtained using relation (4). Both chambers gave consistent values within the limit of their type-A uncertainties, with a ratio of air-kerma rates equal to 1.0038(61). The final value adopted was the average value weighted by the inverse of variances. The relative standard uncertainty of the ratio of current measurements in the eBT and reference beams was of about 0.3%. The results are presented in Table 5.

The source-to-detector distance is here the most important source of uncertainty. For future works it would then be of interest to think about other possible choices for the transfer chamber, by favoring sensitivity rather than energy-response flatness. This would then involve reconsidering the choice of the procedure to follow in step 2.

3.3.3. Air kerma-to-absorbed dose conversion factor

The calculation of the conversion factor F_{KD} was based on the developed Monte Carlo model of the INTRABEAM with a 4 cm spherical applicator. The phsp files defined in section 2.2.3 were used as particle sources in all the calculations. The absorbed dose to water at 1 cm depth in water and the air kerma were both expressed in eV/g per history or primary particle (here, electron emitted toward the gold target). F_{KD} is equal to a ratio of two Monte Carlo calculated dosimetric quantities, the numerator being the absorbed dose to water at 1 cm reference depth in a water phantom, and the denominator the air kerma at the measurement distance in air (at least 10 cm from the source). The value of F_{KD} then results from both a change of medium and a change of distance. In further studies, it could then be advantageously split into two factors specific to each effect, i.e. the ratio of absorbed dose to water to air kerma at the same point (the reference point in water) and the ratio of air kermas at that point and at the point of

measurement in air. Only the last factor would need to be recalculated when changing the measurement distance.

Calculation of the absorbed dose to water at 1 cm depth per history

In the model used for the calculation, the probe covered with its applicator (described in subsection 2.2.3 and figure 3) was placed in the central part of a cylindrical water phantom, large enough to be considered as a full-scatter phantom (20 cm in diameter and 17 cm in height). Two shapes were selected for the absorbed-dose scoring region. The first one was a sphere with its center placed at the reference point in water, i.e. at 1 cm from the applicator surface. The calculation was made with a sphere of 1-mm diameter. The second geometry was a spherical cap, *i.e*. the intersection of a spherical shell of given thickness, concentric to the center of the applicator, and of a cone with an aperture angle defined from the center of the applicator, its midpoint being placed at the reference point in water (see figure 11). The choice of the latter geometry was based on the assumption of the isotropy of the radiation emission from the applicator in the vicinity of the probe axis. It makes possible the use of large volumes to get better statistics, but remaining thin enough to limit the effect of the strong attenuation of photons in water, given their energy. In order to identify possible biases caused by the choice of shell thickness and aperture angle, several simulations were performed, modifying those two parameters. Two shell thicknesses were used, 0.2 mm and 1 mm, associated in the first case with angles of 19° and 45°, and in the second one, with angles of 5.7°, 19° and 45°. No significant bias was observed in the results according to geometry, thickness or angle, statistical uncertainties being larger for smaller volumes (especially the sphere of 1-mm diameter). The absorbed dose to water at the reference point was then derived from the mean of the absorbed doses in those scoring regions, weighted by the inverse of their variances. The result obtained and the associated uncertainties are presented in Table 4. The relative uncertainty due to the

modelled photon-source position corresponds to a length of 0.02 cm on the probe axis, estimated from the hemispherical shape of the target.

Calculation of the air kerma per history

To achieve a reasonable statistical uncertainty in a limited time, the air kerma per history was obtained using the fluence and its energy distribution per initial/primary particle at the point of measurement derived from PENELOPE 2006, and mass energy transfer coefficients of air tabulated as a function of energy.

The scoring region chosen for the calculation was a 1-mm thick spherical cap with a cone angle of 10°, defined as for absorbed dose to water with the same assumption of photon emission isotropy (Figure 5). The parameter E_{abs} was set at 50 keV instead of 1 keV for secondary particles in the lead collimator. The measurement point defined in subsection 3.3.2 was located on the surface of the cap facing the source. The fluence at that point and its energy distribution were derived from the number of photons entering the volume and its energy distribution calculated by PENELOPE 2006. For that, all the photons were assumed to enter through the surface facing the source with a normal incidence. The photons scattered in air entering the scoring volume through its lateral and rear faces were estimated to be negligible. In addition, considering the shape of the surface facing the source, the primary photons emitted from the quasi-point source at the center of the applicator impinge it with a normal incidence. The calculated quantity divided by the area of that surface gave then the fluence at the point of interest.

PENELOPE 2006 having no suitable program to calculate mass energy transfer coefficients, datasets obtained with XMuDat (Nowotny 1998) and EGSnrc (XCOM) ‘g’ application (version V4-r2-4) (Kawrakow et al 2013) were used to evaluate those coefficients for air. Like PENELOPE 2006, those codes do not include the renormalized photoelectrical-effect cross sections reported by ICRU 90 (see ICRU 90, Ch. 6). Their average values weighted by the

photon energy fluences were found consistent, respectively equal to 0.1730 cm^2/g and 0.1732 cm^2/g. For comparison, PENELOPE 2014 (Salvat 2015) which includes renormalized cross sections gives an average mass energy transfer coefficient lower by 2%. This difference is consistent with those reported in (Andreo *et al* 2012) and the ICRU Report 90. The values of the quantities used to get the air kerma per history and the associated uncertainties are presented in Table 4. The uncertainty of the modelled source position is the same as for absorbed dose to water (0.02 cm), with a lower relative value due larger distance.

Resulting value of the conversion factor F_{KD}

Considering the effect of using or not renormalized cross-sections, it can be observed that the difference between calculated ratios of average mass energy transfer coefficients $(\mu_{tr}/\rho)_{water,air}$ is considerably smaller than that of $(\mu_{tr}/\rho)_{air}$ values, due to correlations between dosimetric quantities calculated in air and water. For example, the value of the ratio $(\mu_{tr}/\rho)_{water,air}$ given by PENELOPE 2014 gets very close to those calculated with XMuDat and EGSnrc, with less than 0.1% difference. Then since the calculations of the fluence in air and of absorbed dose to water were made with PENELOPE 2006, the use of datasets of un-renormalized cross-sections for mass energy transfer coefficients in air appeared appropriate, significantly reducing the bias due to the use of un-renormalized data.

For an air kerma at the distance of 13.55 cm, the calculations led to a value of the conversion factor F_{KD} equal to 37.0 with a standard uncertainty of 1.7% (Table 4). This uncertainty value takes into account the reduction of the type-B uncertainty resulting from correlations between the calculated air kerma and absorbed dose to water. They relate to cross sections and to the source position in the probe. A conservative type-B uncertainty of 1% was nevertheless affected to the ratio of the mass energy transfer coefficients, to account for the uncertainty of the energy distributions considering the steep variation of those coefficients in that range of energy.

Table 4. Calculation of the conversion factor F_{KD}.

Calculated quantity	Value	Uncertainty (k=1, %)		
		type A	type B	
		calculation statistics	cross sections, μ_{tr}/ρ	modelled source position
$\overline{(\mu_{tr}/\rho)}_{air}$ (cm^2/g)	0.1731	-	2	
$\bar{\Psi}$ (eV/cm^2/e$^-$)	1.508 10^{-2}	0.7	-	0.3
K_{air} (13.55 cm) (eV/g/e$^-$)	**2.61 10^{-3}**	**0.7**	**2**	**0.3**
D_w (1 cm) (eV/g/e$^-$)	**9.65 10^{-2}**	**0.35**	**2**	**1.3**
F_{KD}	**37.0**	**0.8**	**1***	**1***
		1.7		

*uncertainties excluding components common to K_{air} et D_w (correlations).

3.3.4. Absorbed-dose rate to water at 1 cm depth

The absorbed-dose rate to water at 1 cm depth was calculated using relation (5). The values of the quantities involved and their uncertainties are reported in Table 5. The main uncertainty components come first from the calculated conversion factor F_{KD}, then from the source-detector distance in the air-kerma measurement, and then from the air-kerma reference value.

Table 5. Air-kerma rate measured at 13.55 cm distance from the source and absorbed dose rate to water at 1 cm depth in the eBT beam.

Quantity	Value	Uncertainty (%, k = 1)
$\dot{K}_{air,ref}$ (Gy/s)	3.335 10^{-3}	0.45
k_{dis}	1.000	0.50
k_{stem}	1.008	0.10
$k_{Q,Qref}$	1.000	< 0.10
$I_{TC,eBT}/I_{TC,ref}$ (weighted mean)	3.918 10^{-2}	0.28
$\dot{K}_{air,eBT}$ (mGy/s)	**1.317 10^{-1}**	**0.74**
F_{KD}	**37.0**	**1.7**

$\dot{D}_{w,1\,cm}$ (mGy/s)	4.87	1.9

4. Discussion

4.1. Comparison of measurement results

Zeiss provides for each INTRABEAM system the dose profile in water, for the bare probe, and the transfer functions for spherical applicators. These profiles are updated by Zeiss at each calibration period of the eBT device. Those dose profile data are based on an initial dosimetry method called TARGIT. Its principle relies on measurements made in water with a PTW 23342 chamber calibrated in terms of exposure in a reference beam of close energy, and a dosimetry protocol enabling to express the corresponding calibration coefficient in terms of absorbed dose to water. In 2017, Zeiss started to provide the dose profiles obtained with a new method (V4.0 calibration method) based on the use of a PTW 34013 chamber and a revised dosimetry protocol.

The absorbed-dose rate value obtained in this work was compared with the value provided by the manufacturer for the INTRABEAM system of Saint-Louis Hospital. The manufacturer values considered were extracted from the dose profile database delivered for the bare source with both TARGIT and V4.0 calibration methods and the transfer function of the 4 cm spherical applicator applied to obtain the dose values at 1 cm distance from the applicator surface on the probe axis.

The value determined in the present work was found significantly higher than those provided by Zeiss, by 33% with the TARGIT method and 17% with the second method. Similar works were carried out for bare INTRABEAM sources in other laboratories applying different methods (Schneider 2017, Watson *et al* 2018a, Watson *et al* 2018b). So far they all point out an underestimation of the absorbed-dose rate to water given by the TARGIT method and to a lesser extent by the V4.0 one.

The PTB reported a preliminary work carried out with a standard extrapolation chamber. Their result, given with an uncertainty budget not yet finalized, was found significantly higher than those of the TARGIT and V4.0 calibration methods, respectively by 62% and 22% (Schneider 2017).

More recently, a first publication from McGill University (Watson *et al* 2018a) describes a method based on the calculation, for an ionization chamber calibrated in air kerma in a reference beam of quality Q_0, of a conversion factor C_Q enabling to deduce the calibration coefficient in absorbed dose to water in the measured beam of quality Q. To do so, Monte Carlo models of the source to be characterized (here INTRABEAM) and of the chamber used (here PTW 34013) were developed. Their absorbed-dose values at different depths are compared with those of the manufacturer (V4.0 calibration method). In spite of the uncertainty due to the possible deviation of the actual dimension of the chamber cavity from its nominal value, their results were always higher than the manufacturer ones, with differences at 1 cm depth ranging from 6% to 15%, these extreme values corresponding respectively to the thinner and thicker possible heights of the chamber cavity, given the tolerance associated to its dimension. A second publication by the same laboratory reports the results of a comparison of the TARGIT and V4.0 methods, the C_Q formalism and measurements with calibrated EBT3 Gafchromic films (Watson *et al* 2018b). The TARGIT method gives values lower than those of the V4.0 one, from 14% at 3 cm depth to 60% at 0.5 cm depth. The discrepancies are even larger with the "C_Q formalism" method, from 22% at 3 cm depth to 80% at 0.5 cm depth. The results obtained at 1 cm depth are shown in Table 6. The aim of this table is just to give an overlook of the discrepancies observed between the manufacturer on one side, and the three laboratories on the other side. It is not intended to indirectly compare those laboratories since their results were obtained with different systems, two of them with a bare probe, the third one with an applicator, without any common

protocol of comparison. Nevertheless those results plead for organizing inter laboratory comparisons and establishing international metrological traceability.

Table 6. Measurement results of the absorbed dose rate to water at 1 cm depth compared with those delivered by the manufacturer.

	Irradiation conditions	Ratio to manufacturer's value	
		TARGIT	V4.0
PTB	Bare probe	1.62	1.22
McGill University	Bare probe	1.46*	1.10*
LNE-LNHB	Probe + 4-cm applicator	1.33	1.17

*Values estimated from figure 5 in (Watson et al 2018b).

4.2. Investigation on observed discrepancies

To derive the calibration coefficient of the ionization chamber in terms of absorbed dose to water from that expressed in air kerma, the TARGIT method makes use of the following relation, the reference point C being placed in the chamber cavity on the inner surface of its entrance foil,

$$\frac{N_{\mathrm{D,water}}(\mathrm{C})}{N_{\mathrm{K,air}}(\mathrm{C})} = (\mu_{\mathrm{en}}/\rho)_{\mathrm{water,air}}. \qquad (7)$$

The right-hand term of this relation is equal to the ratio of absorbed dose to water to air kerma at point C when exposed to the same photon fluence in both media, in the absence of chamber. This relation assumes implicitly that the ratio of calibration coefficients does not depend on the chamber.

The ionization chamber used, PTW 23342, has a cavity of 1 mm height and an entrance foil of 30 μm thickness. Considering the energy of electrons set in motion by a 50 kV x-ray beam, the entrance foil can be assumed to be thick enough to ensure charged-particle equilibrium, and the air cavity thin enough to be assimilated to a Bragg-Gray cavity. If so, the absorbed dose in the

cavity should originate exclusively from charged particles created in the entrance foil, and the body of the chamber, mainly the side and back walls surrounding its cavity.

One can then express the absorbed dose to water at point C by the following relation:

$$D_{\mathrm{w}}(\mathrm{C}) = \overline{D}_{\mathrm{air}} \cdot k_{\mathrm{wall,w}} \cdot (\mu_{\mathrm{en}}/\rho)_{\mathrm{w,wall}} \cdot s_{\mathrm{wall,air}} \qquad (8)$$

where $\overline{D}_{\mathrm{air}}$ is the mean absorbed dose in the air cavity, $s_{\mathrm{wall,air}}$ the ratio of mass collision stopping powers in the wall and air, and $k_{\mathrm{wall,w}}$ the correction factor of the photon-fluence perturbation caused by the replacement of water by the wall and body materials in the corresponding volumes. Due to the small size of the cavity and the position of point C, the correction factor for the photon-fluence perturbation caused by the replacement of water by air in the cavity is neglected here.

In the same way, the air kerma can be written for the same chamber, as follows:

$$K_{\mathrm{air}}(\mathrm{C}) = \overline{D}_{\mathrm{air}} \cdot k_{\mathrm{wall,air}} \cdot (\mu_{\mathrm{en}}/\rho)_{\mathrm{air,wall}} \cdot s_{\mathrm{wall,air}} \quad (9)$$

where $k_{\mathrm{wall,air}}$ is the correction factor for the photon-fluence perturbation caused by the replacement of air by the wall and body materials in the corresponding volumes.

The ratio of calibration coefficients can then be written approximately as follows:

$$\frac{N_{D,\mathrm{w}}(\mathrm{C})}{N_{K,\mathrm{air}}(\mathrm{C})} = \frac{k_{\mathrm{wall,w}}}{k_{\mathrm{wall,air}}} (\mu_{\mathrm{en}}/\rho)_{\mathrm{w,air}} \qquad (10)$$

In both media, the effect of the very thin entrance foil should be negligible, but the contribution of scattering and backscattering in the thick back and side plastic walls and the rest of the chamber body has to be examined. The replacement of water with plastic materials should lead to a small perturbation because of to their close atomic numbers and densities, and consequently to a value of $k_{\mathrm{wall,w}}$ close to 1. On the contrary, the replacement of air with this materials can lead to a significant increase of absorbed dose in the cavity, due to particles scattered and backscattered in the body, back and side walls, and thus to a value of the correction factor $k_{\mathrm{wall,air}}$ significantly lower than 1. Finally, the ratio of calibration coefficients can be approximated with the formula:

$$\frac{N_{D,\mathrm{w}}(\mathrm{C})}{N_{K,\mathrm{air}}(\mathrm{C})} \approx \frac{1}{k_{\mathrm{wall,air}}} (\mu_{\mathrm{en}}/\rho)_{\mathrm{w,air}} \qquad (11)$$

The TARGIT expression differs by the absence of the factor $k_{\mathrm{wall,air}}$. This omission should lead to an underestimation of the calibration coefficient in terms of absorbed dose to water.

This conclusion has been confirmed by a Monte Carlo calculation of the effect of the PTW-23342 chamber body when fully irradiated using a simplified geometry. Three materials were introduced, air for the cavity and the medium surrounding the chamber, graphite (1.70 g/cm^3) for the electrodes, and polyethylene (0.94 g/cm^3) for the entrance foil and the chamber body. The correction factor $k_{\mathrm{wall,air}}$ is obtained calculating the ratio of the energies deposited in the air cavity in the absence and presence of the body. In practice, 30 μm-thick walls are introduced in geometry 1, thick enough to ensure charged particle equilibrium but thin enough to make negligible the attenuation of photons. The value of this factor was found equal to 0.873 with a type-A standard uncertainty of 0.64%. The consequence is an increase in the absorbed dose of about 15% compared to the TARGIT method. This result does not fully explain the observed discrepancies and calls for more investigations.

5. Conclusion

The method of dosimetric standardization of eBT systems presented here was tested for an INTRABEAM system and its feasibilty demonstrated. Its applicability to a large variety of eBT devices, in principle possible given the procedure followed, has still to be demonstrated through further experiments with the same device and others.

The results already published by other laboratories and those presented here for the studied eBT system and their comparison with those of the manufacturer clearly highlight absorbed-dose measurement difficulties for such types of device. Some of them can be mentioned here. Interaction coefficients undergo steep variations in function of energy, and from one material to another. They have high values resulting in strong absorbed-dose gradients in water. Reference points are close to the radiation source, thus amplifying the effect of postioning

uncertainty in measurements. In support of the latter consideration, the discrepancies with the values of the manufacturer presented before seem to decrease drastically with increasing distances (for example, see figure 10 in (Watson et al 2018a) and figure 6 in (Watson et al 2018b)).

In addition, given the weight attached to Monte Carlo calculations, e.g. for the evaluatin of the conversion factor from air kerma to absorbed dose to water, the importance of the care to be taken in the different steps has to be highlighted, especially the model used for the eBT system which requires a precise knowledge of the device (energy of electrons, position of bremsstrahlung source, constituent materials, dimensions, etc.), the model of the experimental conditions of measurement (e.g. source-to-detector distance), the adapted choice of calculation parameters.

All those elements call for further studies on the eBT device considered here and others, exchange of information between manufacturers, metrology laboratories and medical physicists, comparisons of absorbed dose measurements and Monte Carlo calculations as well between laboratories based on well defined protocols. The end goal should be to establish international metrological traceability for such eBT devices.

References

Abudra'a A 2017 Development of new dosimetric standards for low energy x-rays (≤ 50 keV) used in radiotherapy *PhD thesis* Université Paris-Saclay

Andreo P, Burns D and Salvat F 2012 On the uncertainties of photon mass energy-absorption coefficients and their ratios for radiation dosimetry *Phys. Med. Biol.* **57** 2117-36

Beatty J, Biggs P J, Gall K, Okunieff P, Pardo F S, Harte K J, Dalterio M J and Sliski A P 1996 A new miniature x-ray device for interstitial radiosurgery : Dosimetry *Med. Phys*. **23** 53-62

Burns D, Roger P, Denozière M and Leroy E 2011 Key comparison BIPM.RI(I)-K2 of the air-kerma standards of the LNE-LNHB, France and the BIPM in low-energy x-rays *Metrologia* **48** *Tech. Suppl.* 06013

Deloule S 2014 Développement d'une méthode de caractérisation spectrale des faisceaux de photons d'énergies inférieures à 150 keV utilisés en dosimétrie *PhD thesis* Université Paris-Sud

Eaton D J and Duck S 2010 Dosimetry measurements with an intra-operative x-ray device *Phys. Med. Biol.* **55** N359-N369

Eaton D J 2015 Electronic brachytherapy-current status and future directions *Br. J. Radiol.* **88** 20150002

Klevenhagen S C, Auckett R J, Harrison R M, Moretti C, Nahum A E and Rosser K E 1996 The IPEMB code for practice for the determination of absorbed dose for x-rays below 300 kV generating potential (0.035 mm Al-4 mm Cu HVL; 10-300 kV generating potential) *Phys. Med. Biol*. **41** 2605-25

Kraus-Tiefenbacher U, Scheda A, Steil V, Hermann B, Kehrer T, Bauer L, Melchert F and Wenz F 2005 Intraoperative radiotherapy (IORT) for breast cancer using the Intrabeam system *Tumori* **91** 339-45

IAEA 2000 Absorbed Dose Determination in External Beam Radiotherapy: An International Code of Practice for Dosimetry based on Standards of Absorbed Dose to Water *IAEA Technical Report Series No 398* (Vienna: International Atomic Energy Agency)

ICRU 2016 Key Data for Ionizing-Radiation Dosimetry: Measurement Standards and Applications (ICRU Report No. 90) (Bethesda, MD: International Commission on Radiation Units and Measurements)

Kawrakow I, Mainegra-Hing E, Rogers D W O, Tessier F and Walters B R B 2013 EGSnrc Code System: Monte Carlo Simulation of Electron and Photon Transport *NRCC Report PIRS-701*

Ma C M, Coffey C W, DeWerd L A, Liu C, Nath R, Seltzer S M and Seuntjens J P 2001 AAPM protocol for 40–300 kV x-ray beam dosimetry in radiotherapy and radiobiology *Med. Phys.* **28** 868-893

Nowotny S 1998 XMuDat: Photon attenuation data on PC *IAEA-NDS-195*

Nwankwo O, Clausen S, Schneider F and Wenz F 2013 A virtual source model of a kilo-voltage radiotherapy device *Phys. Med. Biol.* **58** 2363-75

Plagnard J 2014 Comparison of measured and calculated spectra emitted by the x-ray tube used at the Gustave Roussy radiobiological service *X-Ray Spectrom.* **43** 298–304

Plagnard J 2016 Mesure de spectres en énergie de l'émission de tubes à rayons X au LNE-LNHB/LMD *Revue Française de métrologie* (2016-3) **43** 37-47

Rivard M J, Coursey B M, DeWerd L, Hanson W F, Saiful Huq M, Ibbott G S, Mitch M G, Nath R and Williamson J F 2004 Update of AAPM Task Group No. 43 Report: A revised AAPM protocol for brachytherapy dose calculations *Med. Phys.* **31** 633-674

Salvat F, Fernandez-Varea J M and Sempau J 2006 PENELOPE-2006: A code system for Monte Carlo simulation of electron and photon transport. http://www.oecd-nea.org/science/pubs/2006/nea6222-penelope.pdf

Salvat F 2015 PENELOPE-2014: A Code System for Monte Carlo Simulation of Electron and Photon Transport *NEA/NSC/DOC(2015)3*

Schneider T, Radeck D and Šolc J 2016 Development of a New Primary Standard for the Realization of the Absorbed Dose to Water for Electronic Brachytherapy X-ray Sources *Brachytherapy* **15** S27–S28

Schneider T 2017 Towards reference dosimetry of electronic brachytherapy sources *International Workshop "Metrology for Brachytherapy: state-of-the-art and beyond"* PTB Braunschweig 30-31 May 2017

Seltzer S M, O'Brien M and Mitch M G 2014 New national air-kerma standard for low-energy electronic brachytherapy source *J. Res. Natl. Inst. Stand. Technol*. **119** 554–574

Seuntjens J 2000 AAPM TG-61 report on kilovoltage x-ray dosimetry: II. Calibration procedure and correction factors *Engineering in Medicine and Biology Society. Proceedings of the 22nd Annual EMBS International Conference* vol. 3 IEEE 2313–16

Sievers P, Schneider T, Michel T, and Anton G 2011 X-ray spectroscopy with photon counting imaging detectors such as Timepix *2011 IEEE Nuclear Science Symposium Conference Record* 1826–1828

Sievers P 2012 Time-resolved and position-resolved X-ray spectrometry with a pixelated detector *PhD thesis* Der Naturwissenschaftlichen Fakultät der Friedrich-Alexander Universität Erlangen-Nürnberg ECAP-2012-027

Watson P G F, Popovic M and Seuntjens J 2018a Determination of absorbed dose to water from a miniature kilovoltage x-ray source using a parallel-plate ionization chamber *Phys. Med. Biol.* **63** 015016

Watson P G F, Bekerat H, Papaconstadopoulos P, Davis S and Seuntjens J 2018b An investigation into the INTRABEAM miniature x-ray source dosimetry using ionization chamber and radiochromic film measurements *Med. Phys.* **45** 4274-86

Yanch J C and Harte K J 1996 Monte Carlo simulation of a miniature, radiosurgery x ray tube using the ITS 3.0 coupled electron photon transport code *Med. Phys.* **23** 1551-8

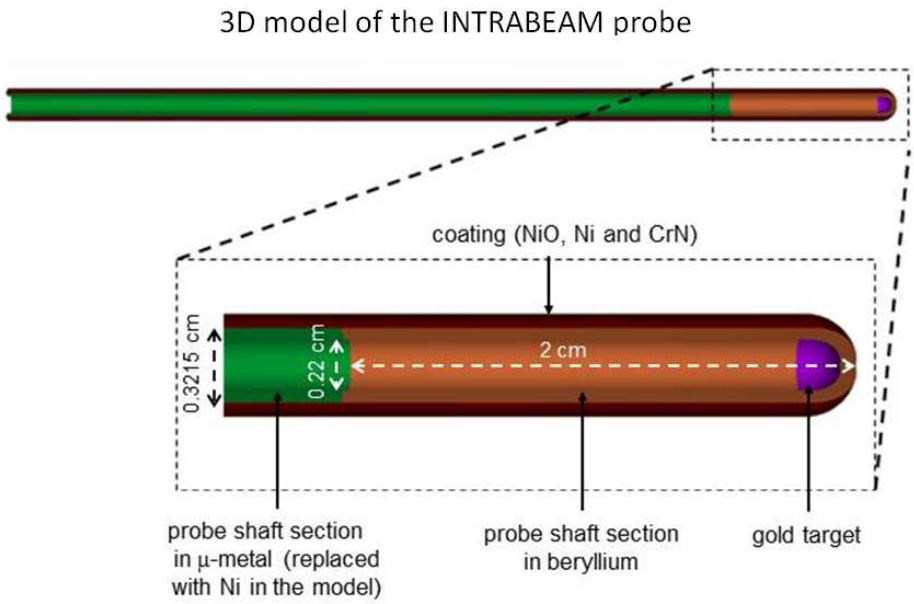

Figure 1. 3D model of the INTRABEAM probe obtained using the geometry viewer tool of PENELOPE (sectional view with intersecting planes at 90°).

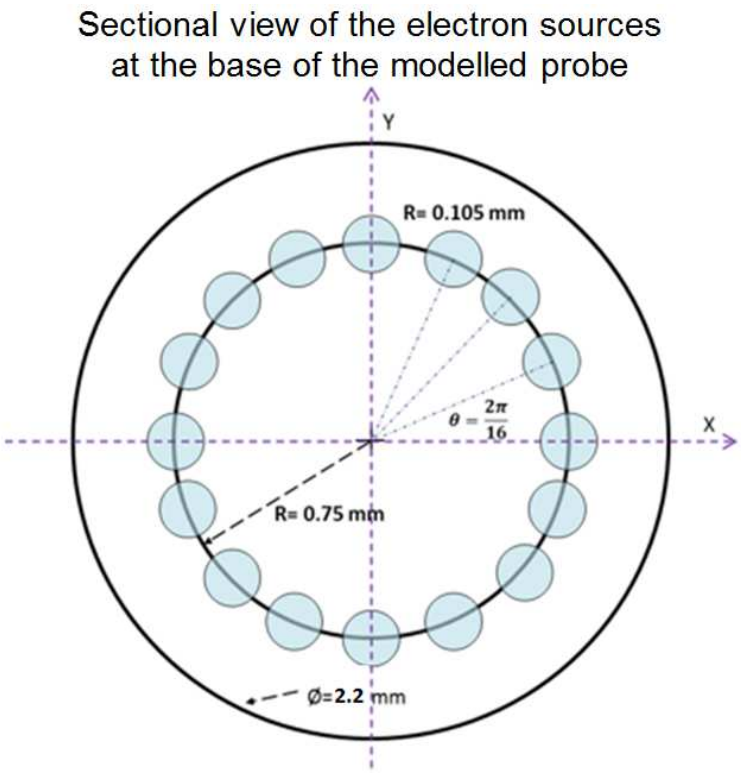

Figure 2. Scheme (not to scale) of the 16 disk-shaped electron sources located at the base of the modelled probe in the Monte Carlo model.

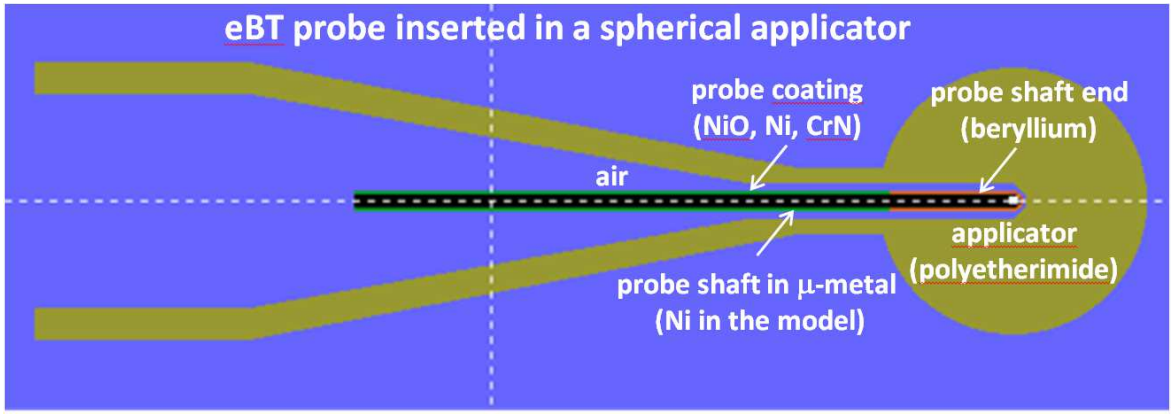

Figure 3. PENELOPE geometrical model of the probe inserted in the spherical applicator in materials view mode (gview2D program).

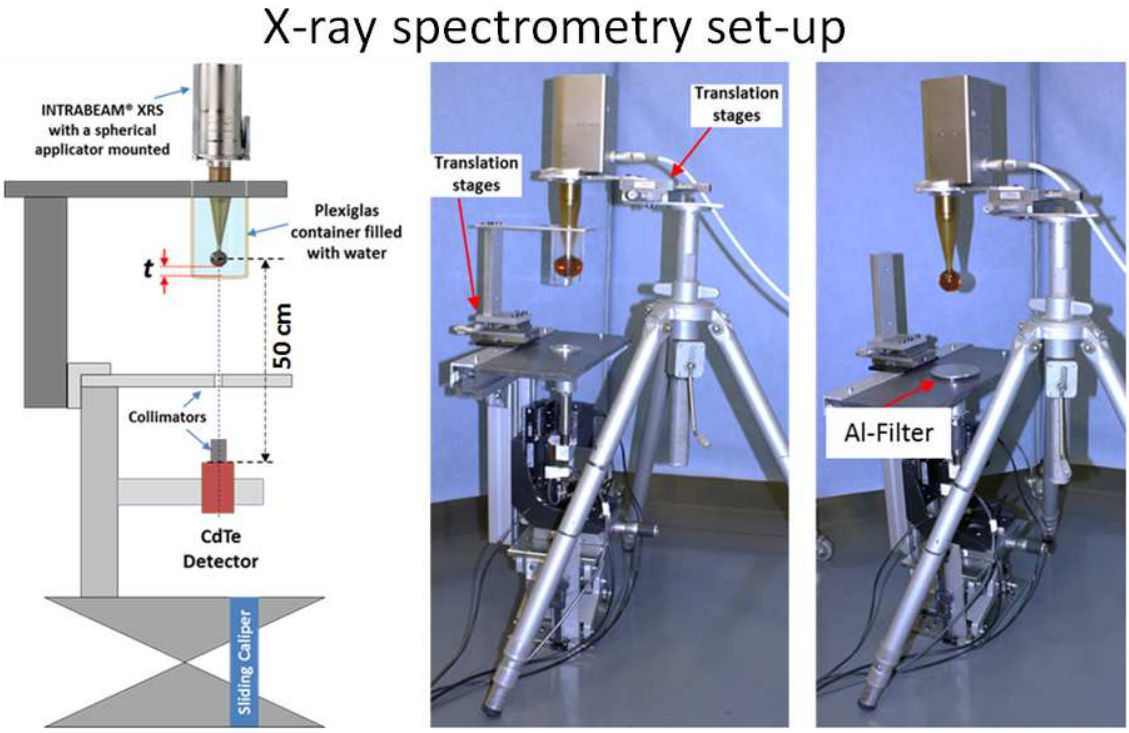

Figure 4. Spectrometry setup configurations: (left) scheme (not to scale) of the developed system with Plexiglas container filled with water, (middle) picture of the real system used for photon spectra measurements, and (right) picture of the same system with an Al filter of adequate thickness to replace the water-filled container.

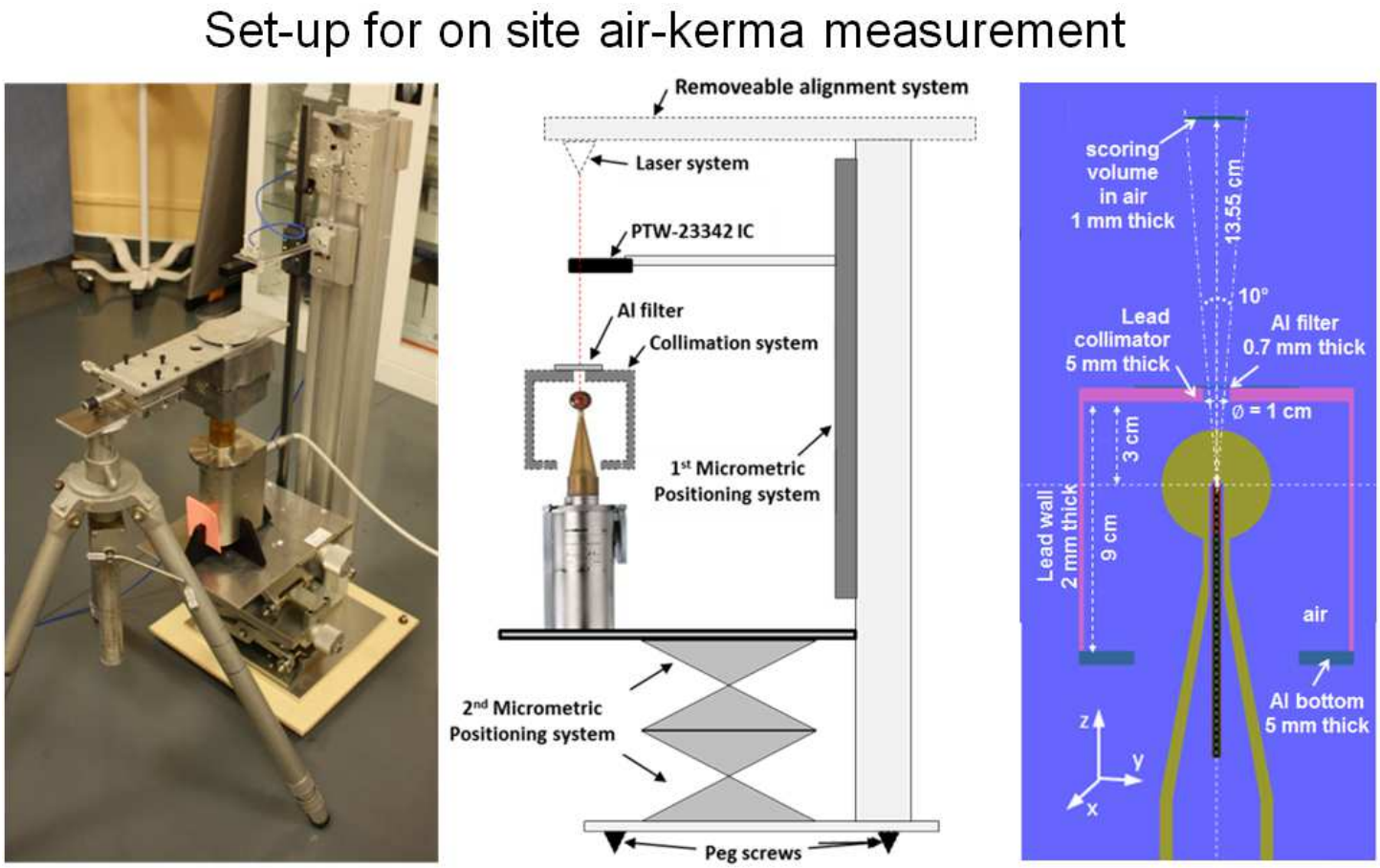

Figure 5. Measurement set-up for the on-site characterization in air-kerma rate of an INTRABEAM x-ray source with applicator using a calibrated PTW 23342 chamber. Left and middle: picture and scheme not to scale. Right: Monte Carlo model (sectional view).

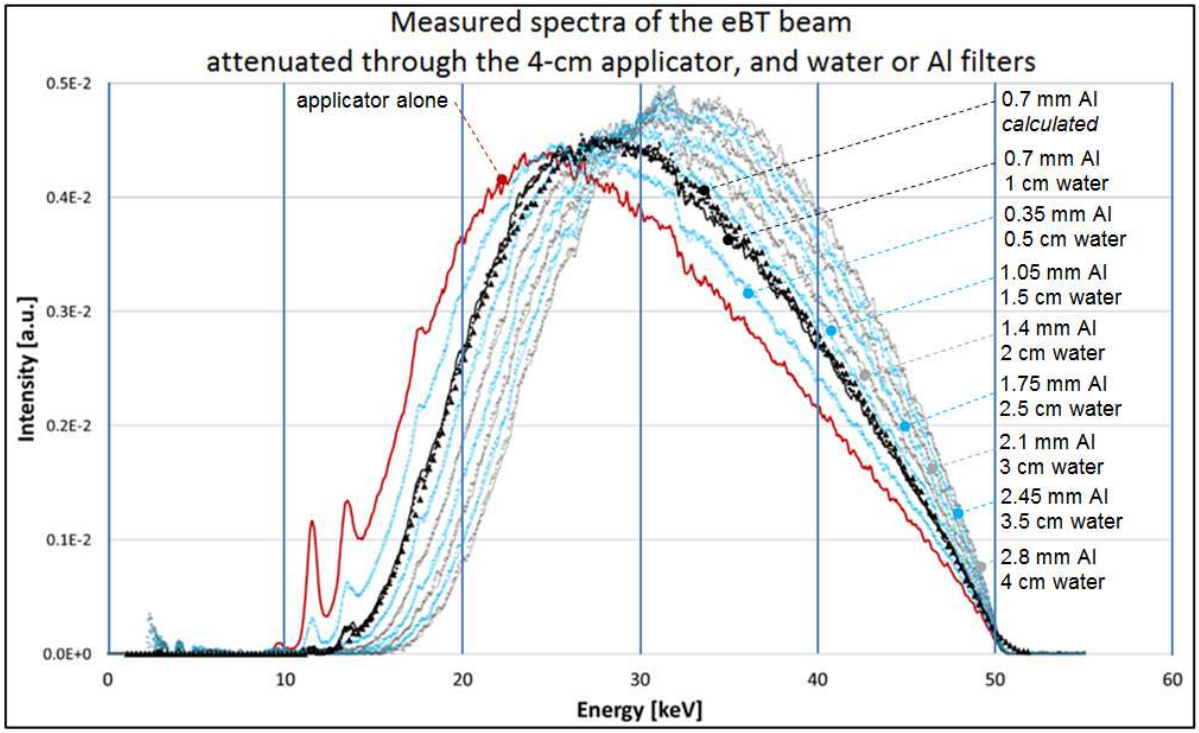

Figure 6. Evolution of measured spectra of the INTRABEAM source with the 4 cm applicator (normalized to surface area) for increasing attenuations. Red line: applicator alone. Open circles: immersed in a container filled of water. Continuous lines: in air with Al filters. Black open circles and line: measured spectra with respectively 1 cm of water and 0.7 mm of Al. Black triangles: calculated spectrum with 0.7 mm Al filtration. Superimposed spectra correspond to equivalent filtrations in water and Al.

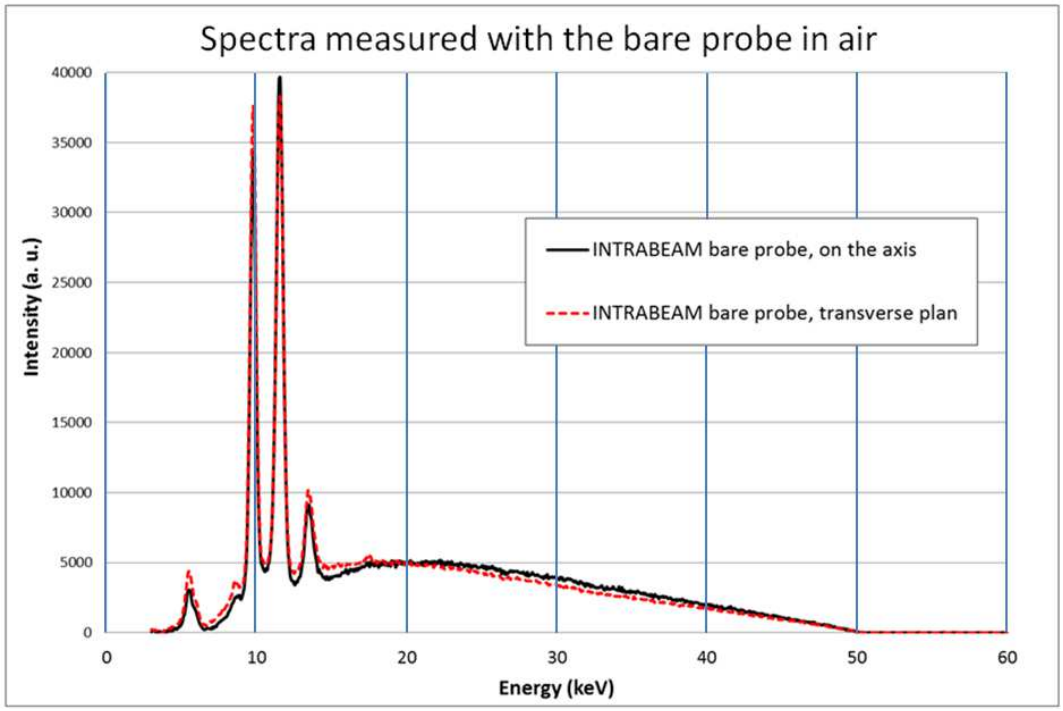

Figure 7. Surface-area-normalized photon energy spectra measured for the INTRABEAM bare probe in air on the probe axis and on the transverse plane of the probe tip, with the gold L-fluorescence peaks in the low-energy region.

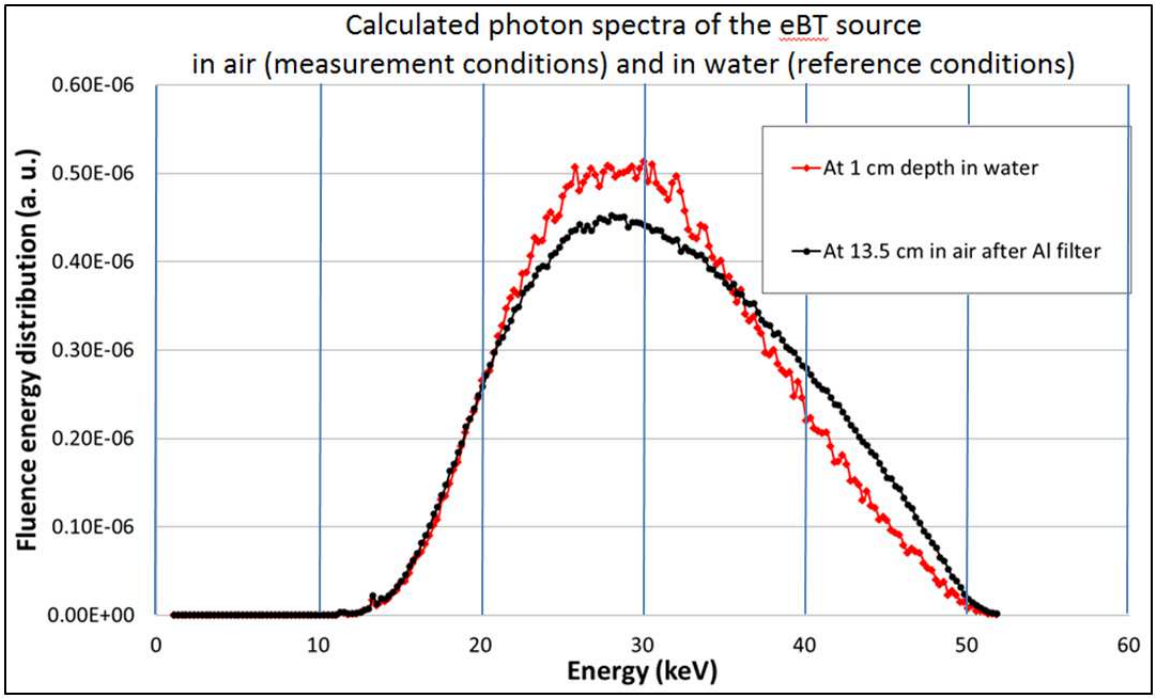

Figure 8. Surface-area-normalized photon spectra calculated at the reference points on the probe axis, in air (4 cm applicator and 0.7 mm Al filter, probe tip distance of 13.5 cm) and water (4 cm applicator, 1 cm water depth in a water phantom).

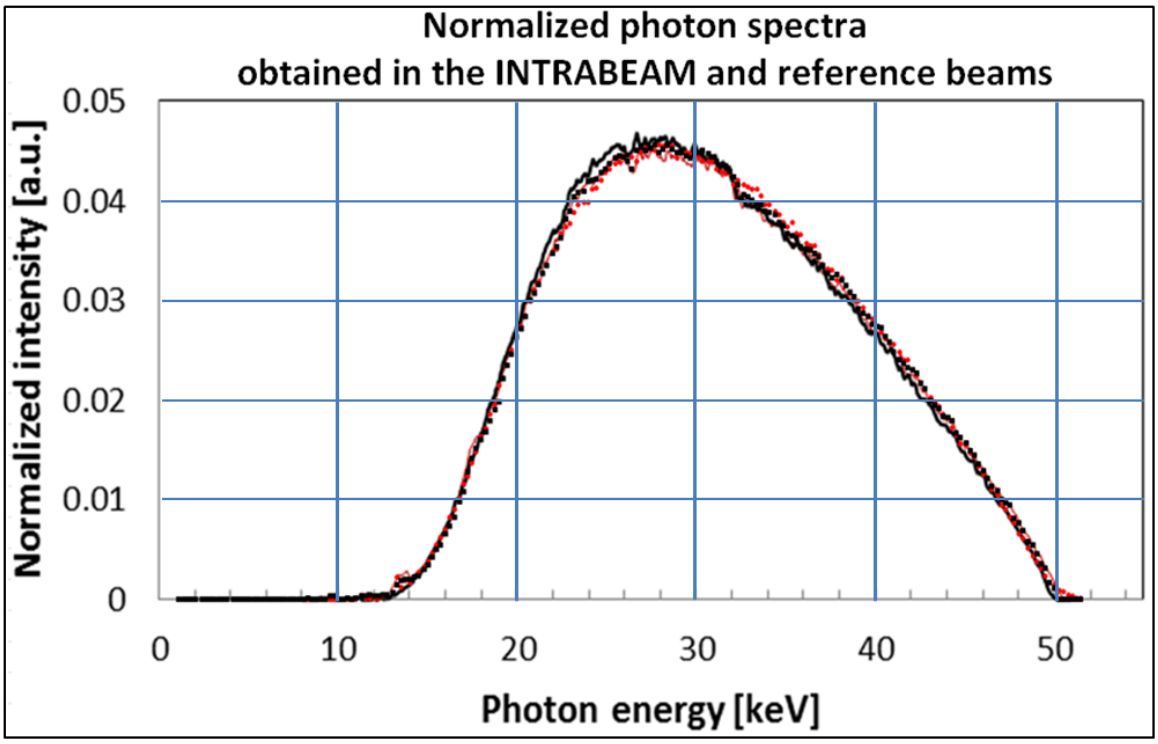

Figure 9. Surface-area-normalized INTRABEAM spectra with a 4 cm applicator and a 0.7 mm aluminum filter, measured (red line) and calculated (red dots), compared with those of the reference x-ray generator, measured (black line) and calculated (black dots).

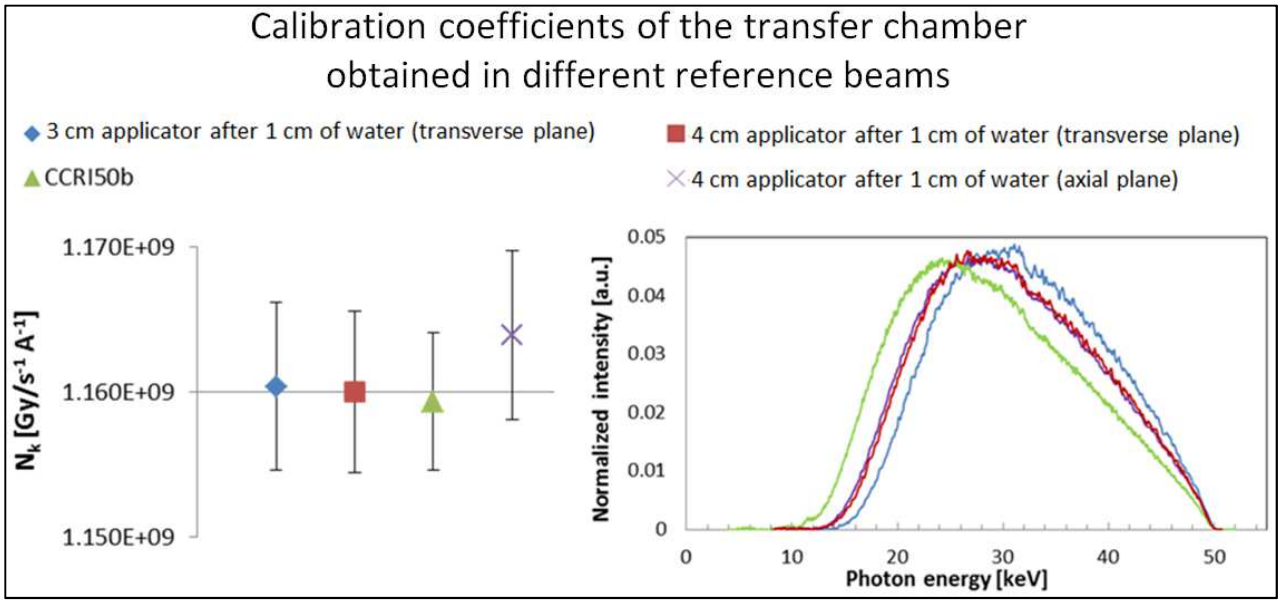

Figure 10. Comparison of the calibration coefficients obtained for a PTW-23342 chamber in reference beams with different photon energy spectra. Uncertainty bars (left) represent type-A standard uncertainties.

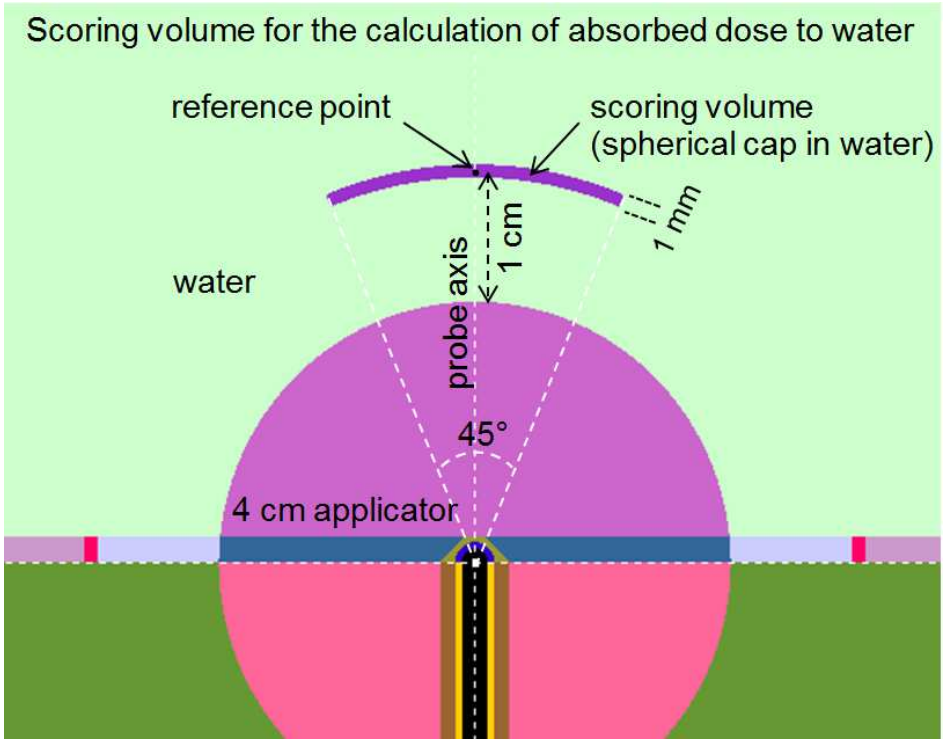

Figure 11. Sectional view (PENELOPE geometrical model) of a scoring volume surrounding the reference point (at 1 cm depth in water, on the probe axis): 1-mm thick spherical cap with a 45° cone angle. The center of the applicator and those of the two spheres delimiting the cap are superposed.